FIXED POINT METHODS AND OPTIMIZATION
Volume 1 (2024), No. 1, 31–46
https://doi.org/10.69829/fpmo-024-0101-ta03
Tulipa Opera Scholarum

OVERLAPPING GRID MULTIDOMIAN SPECTRAL QUASILINEARIZATION METHOD FOR WILLIAMSON NANOFLUID WITH GYROTACTIC MICROORGANISMS FLOW PAST A RADIALLY STRETCHING SHEET

THOKOZANI N. KHUMALO[1,*], MEKONNEN S. AYANO[1], AND VUSI M. MAGAGULA[1]

[1] *Department of Mathematics, University of Eswatini, Private Bag 4, Kwaluseni M201, Eswatini*

Abstract. In this paper, magnetohydrodynamic (MHD) heat and mass transfer of bioconvective Williamson nanofluid flow over a radially stretching sheet is studied. Microorganisms are used to stabilize the suspended nanoparticles through bioconvection. The nanoparticles are accounted for using the Brownian motion and thermophoretic phenomena. By establishing suitable similarity variables, the governing nonelinear partial differential equations modeling the flow are transformed into nonlinear systems of ordinary differential equations (ODE's), which are then solved numerically using the recently developed overlapping grid multidomian spectral quasilinearization method (OGMDSQLM) on MATLAB. The effect of various physical parameters on the flow profiles is investigated graphically and in tables. Amongst other findings, it is found that increasing the radiation parameter augments the temperature profile, while the concentration of microorganisms profiles decline with a rise in the value of the chemical reaction parameter.

Keywords. Quasilinearization, OGMDSQLM, Williamson fluid, radiation, nanofluid, chemical reaction.

1. Introduction

In recent years, the study of nanofluids coupled with microorganism transport has attracted considerable attention due to its relevance in various engineering and biological applications. Understanding the behavior of such complex fluid systems is crucial for optimizing processes in fields ranging from biomedical engineering to environmental science, for instance. Addition of nanometre size metallic or non-metallic particles in a base fluid (such as water, oil and ethyl glycol), results in a mixture called a nanofluid. The notion of nanofluid was coined by [5, 32] and they were the first to bring to the attention of the scientific community the heat transfer consequences of nanofluids. Choi and Eastman concluded that a very small volume fraction (as little as 1%) of nanoparticles added to a base fluid lead to a significant increase in the effective thermal conductivity of the base fluid [5]. The non-homogenous Buongiorno model attributes this enhancement of thermal conductivity to Brownian motion and thermophoretic diffusion of nanoparticles [4]. These fluids have attracted tremendous research interest and a range of applications, considering various flow regimes (two-dimensional heat and mass transfer boundary layer flow over stretching or shrinking sheets, porous media, for instance).

As fixed-point techniques are essential for resolving iterative systems and nonlinear equations that are frequently encountered in the study of fluid dynamics and nanofluid behavior, Fixed-point methods iteratively apply a transformation on an initial guess with the goal of convergently arriving at a solution satisfying a specific system of equations. Numerical simulations of Williamson nanofluids could be

*Corresponding author.
E-mail addresses: thokozanik74@gmail.com (T. N. Khumalo), msayano@uniswa.sz (M.S. Ayano), and gutjwaw@gmail.com (V. M. Magagula)
2020 Mathematics Subject Classification: 60J65; 60J70; 80A19;
Accepted: May 17, 2024.

made more accurate and performance by using optimization approaches. We maximize specific objective functions or restrictions by rephrasing the issue as an optimization work, which raises the overall effectiveness and dependability of the simulations [29]. Adjusting the settings of the multidimensional spectral quasi-linearization approach for the optimal results can be done with common optimization algorithms like gradient descent, genetic algorithms, and simulated annealing. Broadly speaking, a comprehensive approach to the analysis and optimization of Williamson nanofluid behavior can be obtained by integrating the multidimensional spectral quasi-linearization method with optimization techniques and fixed point methods; see [29, 11, 14].

Two-dimensional heat and mass boundary layer flow over stretching sheets applications include, engineering processes, such as, extraction of polymer sheets, wire drawing, paper production and fibreglass production [24]. The problem of two-dimensional flow due to a stretching sheet was first formulated by Crane [6]. Crane reported an exact similarity solution in closed form of this two-dimensional problem [6]. In recent studies, Tamizharasi [31] studied the pressure in a steady two-dimensional MHD flow of viscous incompressible fluid over a flat stretching sheet and reported a finite pressure distribution. The transition effect of boundary layer flow with and without influence of magnetic field for steady and unsteady flow over linearly stretching sheets along the direction of the fluid flow was examined by Kumaran [12, 13]. Shawky [26] studied MHD Williamson nanofluid flow over a stretching sheet in a porous media and reported that an increase in the Brownian motion parameter results in a decrease of the nanoparticle concentration profile. Some studies involving nanofluid flow through porous media can be found in the work of [33, 16, 20, 23, 17]. Even though nanofluids have been reported to possess superior heat transfer characteristics to traditional base fluids, the nanoparticles are usually not stable in the fluid [24, 25]. Furthermore, there is no universal mathematical model for nanofluids. Nevertheless, incorporation of motile microorganisms in the fluid are some of the efforts whose objective is to improve the stability of nanoparticles [6]. The idea with the use of microorganisms to improve stability of nanoparticles is to take advantage of the bioconvection phenomenon [8]. A comprehensive review on bioconvection can be found in [7]. Recently, hybrid nanofluids are being considered to address some of the identified challenges of nanoparticles in a base fluid [25].

The Williamson fluid model considers non-Newtonian behaviour in shear thinning fluids. First suggested by Williamson [34], this model, amongst other models, has been adopted by many researchers in numerical investigation of nanofluids [22, 27, 30]. Ayano et al. [2] investigated the effect of the Hall parameter on the flow over a stretching boundary in a porous medium of a Casson fluid in which gyrotactic microorganisms have been added. In this study they concluded that, a decrease in the Hall parameter results in an increase in the heat transfer rate, the mass transfer rate, and the density of the motile microorganisms, while on the other hand, increasing the porosity parameter reduces the skin friction, heat transfer rate, mass transfer rate, and density of the motile microorganisms. Ibrahim and Gamachu [9] used the spectral quasilinearization method to find numerical solutions to arising model equations for a nonlinear convection steady, laminar flow of an electrically conducting Williamson nanofluid past a radially stretching sheet with an electric field applied transverse to the flow. Their main findings include, augmentation of the velocity profile when the electric field, buoyancy and nonlinear convection parameters grow in value [9]. Atif, Hussein and Sagheer [1] considered numerical analysis of two-dimensional bioconvective MHD mixed convection flow over a stretching sheet of a micropolar nanofluid. Some of their results indicate increasing microorganism density profile and reduced velocity profile when the buoyancy ratio parameter is enhanced [1]. Using the Buongiorno model to account for Brownian motion and thermophoresis, numerical results on Williamson nanofluid boundary layer flow past a stretching sheet with velocity and thermal slips are presented by Bing Kho et al. [3]. Their results depict decreasing boundary layer as the slip parameters increase in value. Furthermore, they (Bing Kho et al.) report enhanced temperature and concentration profiles as the Williamson parameter is increased [3]. The effect of viscous dissipation on unsteady two-dimensional boundary layer

flow of Williamson nanofluid with thermal radiation and chemical reaction, past a stretching/shrinking inclined sheet is presented by Ibrahim and Negera [10]. An upsurge of the inclination angle and unsteady parameter resulted in an increase of the velocity profile, while the velocity profile diminished with an increase in Williamson parameter [10]. A recent study by Zhang et al.[36] focuses on MHD bioconvective Williamson fluid flow past a stretching vertical cylinder, highlighting a decrease in the fluid velocity and momentum boundary layer when the magnetic parameter is increased, while the distribution of microorganisms in the fluid varied inversely with the Pecelet number, amongst other observations on the flow profiles [36].

The combination of nanofluids, which are colloidal suspensions containing nanoparticles, and microorganisms, such as gyrotactic microorganisms, introduces unique challenges to fluid dynamics analysis. These challenges stem from the interactions between fluid flow, heat transfer, nanoparticle dynamics, and microorganism behavior, all of which occur simultaneously and influence each other. Furthermore, considering practical applications, the geometry of the flow domain may be complex, requiring sophisticated numerical techniques for accurate modeling. In this context, the present study focuses on the application of OGMSQM [15] to investigate the flow characteristics of Williamson nanofluid with gyrotactic microorganisms past a radially stretching sheet. The OGMSQM approach offers several advantages for tackling the complexities inherent in this problem. By employing overlapping grids and spectral methods, the computational domain can be discretized efficiently while accurately capturing the intricate features of the flow. The quasilinearization technique further enhances the computational efficiency by iteratively solving the nonlinear governing equations, thereby reducing computational costs without compromising accuracy.

Inspired by the above works, [34, 35, 36] through this article we aim to provide a comprehensive overview of the OGMSQM methodology and its application to the study of Williamson nanofluid with gyrotactic microorganisms flow past a radially stretching sheet. By elucidating the underlying principles, numerical techniques, and computational results, we seek to contribute to the advancement of understanding in this interdisciplinary field, with implications for both engineering and biological sciences. To the best of the authors' knowledge, in the existing literature a comprehensive study for bioconvective Williamson nanofluid flow over a stretching sheet considering radiation, chemical reaction, thermophoresis with slip effects not addressed. The modeled problem yield nonlinear systems of ODE's that is solved numerically using the overlapping grid multidomian spectral quasilinearization method.

2. Model description and mathematical formulation

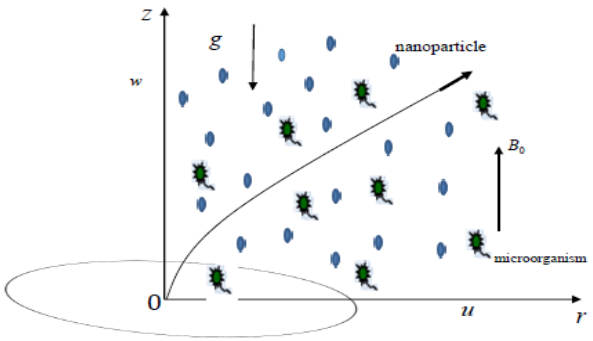

Figure 1. Flow geometry

We considered steady, two-dimensional, incompressible viscous, MHD Williamson nanofluid flow embedded in a medium filled with fluid in a suspension of gyrotactic microorganisms over a radially

stretching plate. The sheet is stretching linearly with a velocity $U_{w(r)} = ar$ in the $r-$direction as shown in Figure 1, where a is a non-negative rate of stretching of the surface. A uniform strength of magnetic field B_o is applied perpendicular to the flow direction (parallel to z axis) and small magnetic Reynolds number is assumed so that the induced magnetic field is neglected. At the surface prescribed temperature or heat flux, velocity and thermal slip is assumed. The temperature variation is assumed sufficiently weak so that it does not kill microorganisms and gyrotactic behavior. Furthermore, density differences in the fluid are taken to be negligible so that the Boussinesq approximation is valid in the mathematical model. In the Cauchy stress tensor equation [28], the extra stress tensor $\mathbf{S}$ for a Williamson fluid is defined as shown in Equation 2.1 [34]. The parameters μ_0, μ_∞, $\Gamma > 0$ and the matrix vector $\mathbf{A}_1$ in (2.1) represent the limiting viscosity at zero (0) shear rate, limiting viscosity at infinite shear rate, a time constant and the Rivlin-Erickson stress tensor, respectively [9].

$$\mathbf{S} = \left[\mu_\infty + \frac{\mu_0 - \mu_\infty}{1 - \Gamma\dot{\gamma}}\right]\mathbf{A}_1 \tag{2.1}$$

The shear rate is given by (2.2), where π is the second invariant of strain rate tensor

$$\dot{\gamma} = \sqrt{\frac{\pi}{2}}, \quad \text{where} \quad \pi = \frac{1}{2}trace(\mathbf{A}_1^2) \tag{2.2}$$

Considering the Williamson fluid constitutive equation for $\mu_\infty = 0$ [34, 9], (2.1) reduces to (2.3).

$$\mathbf{S} = \left[\frac{\mu_0}{1 - \Gamma\dot{\gamma}}\right]\mathbf{A}_1 \tag{2.3}$$

A binomial expansion of $\frac{1}{1-\Gamma\dot{\gamma}}$, taking $\Gamma\dot{\gamma} \ll 1$, so that higher order terms can be neglected in the formulation, is shown in (2.4).

$$\frac{1}{1 - \Gamma\dot{\gamma}} = \sum_{n=0}^{\infty}(\Gamma\dot{\gamma})^n = 1 + \Gamma\dot{\gamma} + (\Gamma\dot{\gamma})^2 + \cdots \tag{2.4}$$

From (2.4), neglecting higher order terms, the extra stress tensor for a pseudoplastic fluid can be approximated by (2.5).

$$\mathbf{S} \approx \mu_0(1 + \Gamma\dot{\gamma})\mathbf{A}_1 \tag{2.5}$$

Following the above constraints, formulation and the work of [9], the governing equations for the model considered are outlined in (2.6)-(2.10).

$$\frac{\partial u}{\partial r} + \frac{u}{r} + \frac{\partial w}{\partial z} = 0 \tag{2.6}$$

$$u\frac{\partial u}{\partial r} + w\frac{\partial u}{\partial z} = \frac{\mu}{\rho}\frac{\partial^2 u}{\partial z^2} + \Gamma\nu\left(\frac{\partial u}{\partial z}\right)\left(\frac{\partial^2 u}{\partial z^2}\right) + g(\beta_t(T - T_\infty) - \gamma_w\triangle\rho n) - \frac{\sigma B_0^2}{\rho}u \tag{2.7}$$

$$u\frac{\partial T}{\partial r} + w\frac{\partial T}{\partial z} = \frac{k}{\rho C_p}\frac{\partial^2 T}{\partial z^2} + \tau\left[D_B\frac{\partial C}{\partial z}\frac{\partial T}{\partial z} + \frac{D_T}{T_\infty}\left(\frac{\partial T}{\partial z}\right) - \frac{1}{\rho C_p}\frac{\partial q_r}{\partial z} + \right] + \frac{\sigma B_0^2}{\rho C_p}u^2 \tag{2.8}$$

$$u\frac{\partial C}{\partial r} + w\frac{\partial C}{\partial z} = D_B\frac{\partial^2 C}{\partial z^2} + \frac{D_T}{T_\infty}\frac{\partial^2 T}{\partial z^2} - k_1(C - C_\infty) \tag{2.9}$$

$$u\frac{\partial n}{\partial r} + w\frac{\partial n}{\partial z} = D_m\frac{\partial^2 n}{\partial z^2} - \frac{bw_c}{C_w - C_\infty}\frac{\partial}{\partial z}\left(n\frac{\partial C}{\partial z}\right) \tag{2.10}$$

The boundary conditions for the governing equations are [1]:

$$u(r,z) = U_w(r) + A\frac{\partial u}{\partial z}, \quad w(r,z) = 0, \quad -k\frac{\partial T}{\partial y} = h_f(T_f - T), \quad C = C_w \quad n = n_w, \quad \text{at} \quad z = 0$$

$$u(r,z) \to 0; \quad w \to 0; \quad T \to T_\infty, \quad C \to C_\infty, \quad \text{as} \quad z \to \infty. \quad n \to n_\infty, \quad \text{as} \quad z \quad \to \infty \tag{2.11}$$

In (2.6), q_r is the Rosseland radiative heat flux and is defined in (2), where σ^* is the Steffen-Boltzmann constant and k^* is the mean absorption coefficient.

$$q_r = -\frac{4\sigma^*}{k^*}\frac{\partial T^4}{\partial r} \tag{2.12}$$

Assuming the difference between the temperature value close to the boundary (T) and far away from the boundary (T_∞) is small, T^4 in (2) is linearized using Taylor series about T_∞ as shown in (2). In (2.6), n represents the density of motile microorganisms, b is the chemotaxis constant, w_c is the maximum speed of microorganism in the fluid, D_m is the microorganism diffusion coefficient, $\frac{bw_c}{C_w - C_\infty}\partial C$ is the velocity related to microorganism swimming.

$$T^4 = T_\infty^4 + \frac{4T_\infty^3}{1!}(T - T_\infty) + \frac{12T_\infty^2}{2!}(T - T_\infty)^2 + \frac{24T_\infty}{3!}(T - T_\infty)^3 + \cdots \tag{2.13}$$

The acceleration due to gravity is denoted with g in the momentum equation ((2.6)), u, w are the velocity components of the flow along the r and z directions, respectively, T is the temperature, C is the nanoparticles volume fraction, Γ is is a time constant,

β_T is the coefficient of thermal expansion, $\triangle\rho$ is the density difference between a cell and fluid, T_∞ is reference temperature, C_∞, n_∞ is the reference concentration of nanoparticles and reference concentration of the microorganisms, respectively, D_T and B_D are the coefficient of thermophoretic diffusion and Brownian diffusion, respectively, $\tau = \frac{(\rho c)_p}{(\rho c)_f}$ is the ratio of heat capacity of nanofluid to base fluid, σ is electric conductivity and B_0 is a constant Magnetic field.
The governing partial differential equations are then transformed into a system of ordinary differential equations (2.17)-(2.18) using the similarity variables (2).

$$\begin{gathered} u(r,z) = arf'(\eta),\ w(r,z) = -2\sqrt{a\nu}f(\eta),\ T - T_\infty = \theta(T_f - T_\infty), \\ C - C_\infty = \phi(C_w - C_\infty),\ n - n_\infty = \chi(n_w - n_\infty),\ \eta = \sqrt{\frac{a}{nu}}z \end{gathered} \tag{2.14}$$

$$f'''\left(1 + Wef''\right) + ff'' - f'^2 + \lambda(\theta - Ra_b\chi) - Mf = 0 \tag{2.15}$$

$$\frac{1}{Pr}\left(1 + \frac{4}{3}R_d\right)\theta'' + N_b\phi'\theta' + N_t\theta'^2 + 2f\theta' = 0 \tag{2.16}$$

$$\phi'' + 2LePrf\phi' + \frac{Nt}{Nb}\theta'' - LeK\phi = 0 \tag{2.17}$$

$$\chi'' + S_b\chi' f' - Pe\chi'\phi' Pe(\chi - B)\phi' = 0 \tag{2.18}$$

Following the transformation of PDE's to ODE's above, the boundary conditions become (see Equations 19):

$$\begin{gathered} f = 0, \quad f' = 1 + \gamma f'', \quad \theta' = -B_t(1 - \theta), \quad \phi = 1, \quad \chi = 1, \text{ at} \quad \eta = 0 \\ f' \to 0, \quad \theta \to 0, \quad \phi \to 0, \quad \chi \to 0, \quad \text{as} \quad \eta \to \infty. \end{gathered} \tag{2.19}$$

Referring to the system ODE's and the associated boundary conditions above, $\lambda = \frac{G_{r(r)}}{Re_r}$ is mixed convection parameter, $G_{r(r)} = (g\beta_t(T_f - T_\infty)r^3)/\nu^2$ is local Grashoff number, $Re_r = aU_w/\nu$ is local Reynolds number, $M = \sigma B_0^2/a\rho$ is magnetic parameter, $Rd = 4\sigma^* T_\infty^3/kk^*$ is radiation parameter, $K = k/\alpha a$ is chemical reaction parameter, $Pe = bWe/D_n$ is Peclet number, $S_b = \nu/D_n$ is the Schmidt number, $Nt = \tau D_T(T_f - T_\infty)/T_\infty\nu$ is thermophoresis parameter, $Nb = \tau D_B(C_w - C_\infty)$ is Brownian motion,$B_t = \frac{a}{\nu}h_f$ is Biot number, $\gamma = A\sqrt{a\nu}$ is first order slip.

Physical quantities of engineering interest considered in this study are, the skin friction (C_f), the Nusselt number (Nu) and the Sherwood number (Sh), defined as shown in (2), where τ_{wr}, q_w and j_m are expressed in (2).

$$C_f = \frac{\tau_{wr}}{\frac{1}{2}\rho(ar)^2},\ Nu_r = \frac{q_w}{k(T_f - T_\infty)},\ Sh_r = \frac{j_m}{C_w - C_\infty} \tag{2.20}$$

where;

$$\tau_{wr} = \mu\left[\frac{\partial u}{\partial z} + \frac{\Gamma}{\sqrt{2}}\left(\frac{\partial u}{\partial z}\right)^2\right]_{z=0},\ q_w = -k\left(\frac{\partial T}{\partial z}\right)_{z=0},\ j_m = -D_B\left(\frac{\partial C}{\partial z}\right)_{z=0} \tag{2.21}$$

Using (2) the dimensionless form of skin friction, local Nusselt number, local Sherwood number become (see (2.22)):

$$C_f Re_r^{1/2} = 2\left(1 + \frac{We}{2}f''(0))f''(0)\right),\ Nu_r Re_r^{-1/2} = -\theta'(0),\ Sh_r Re_r^{-1/2} = -\phi'(0) \tag{2.22}$$

3. Implementation of the numerical method

Numerical solutions were then found using the overlapping grid multidomain spectral quasilinearization method, which was developed by Mkhatshwa M. P. [15]. The solution algorithm of the overlapping grid multidomain spectral quasilinearization method utilizes the following ideas that are prominent in numerical approximation of solution: quasilinearisation method (QLM), spectral collocation, multidomain overlapping grid and Lagrange interpolation polynomials with Gauss-Lobatto discretization. Essentially, the overlapping grid spectral quasilinearization method is dividing the domain of integration ($[0, \eta_\infty]$), into finite overlapping subintervals of equal length as shown in Figure 2 [15]. As shown in this figure, the domain of integration is divided into $p \in \mathbb{N}$ subintervals, with each subinterval further discretized into $N_\eta + 1$ collocation points. The spectral quasilinearization method (SQLM) [18] is then applied in each subinterval, with the approximate solution(s) of a previous subinterval set as starting values for SQLM iterations in the next interval. Below, the system of nondimensional differential equations, as well as the boundary conditions, are conveniently written with subscripts l (see (3.1)-(3.4)), which denotes a subinterval, in order to provide some main steps of the numerical method as applied in this present study. For rigorous details and background on this method, reference is made to [15].

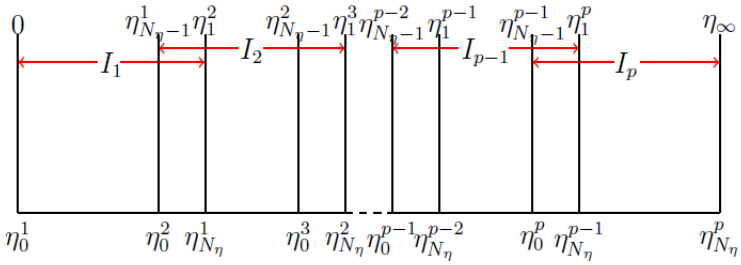

Figure 2. Overlapping grid [15].

$$f_l''' + We f_l'' f_l''' + 2f_l f_l'' - f_l'^2 + \lambda\left[\theta - Nr\phi - Rb\chi\right] - M f_l' = 0 \tag{3.1}$$

$$\theta_l'' + PrNb\theta_l'\phi_l' + PrNt\theta_l'^2 + 2Pr f_l\theta_l' + Rd\theta_l'' = 0 \tag{3.2}$$

$$\phi_l'' + 2LePr f_l\phi_l' + \frac{Nt}{Nb}\theta_l'' - LeK\phi_l = 0 \tag{3.3}$$

$$\chi_l'' + Sb\chi_l f_l - Pe\chi_l'\phi_l' - Pe\left[\chi_l + B\right]\phi_l' = 0 \tag{3.4}$$

The boundary conditions for (3.1)-(3.4) then become

$$\begin{aligned} f_l(\eta) = 0, \quad f_l'(\eta) = 1 + \gamma f_l'', \quad \theta_l'(\eta) = -Bt\left(1 - \theta_l(\eta)\right), \\ \phi_l(\eta) = \chi_l(\eta) = 1 \quad \text{at} \quad \eta = 0 \\ f_l'(\eta) \to 0, \quad \theta_l(\eta) \to 0, \quad \phi_l(\eta) \to 0, \\ \chi_l(\eta) \to 0, \quad \text{as} \quad \eta \to \infty. \end{aligned} \tag{3.5}$$

3.1. **Implementation of the overlapping grid multidomian spectral quasilinearization method.** Using the QLM scheme, the linearized form of (3.1)-(3.4) is shown below (3.6).

$$\left\{\begin{array}{r} a_{1,1}^{(3,l)} f_{l(r+1)}''' + a_{1,1}^{(2,l)} f_{l(r+1)}'' + a_{1,1}^{(1,l)} f_{l(r+1)}' \\ + a_{1,1}^{(0,l)} f_{l(r+1)} + a_{1,2}^{(0,l)} \theta_{l(r+1)} + a_{13}^{(0,l)} \phi_{l(r+1)} + a_{14}^{(0,l)} \chi_{l(r+1)} = R_{1,l} \\ a_{2,2}^{(2,l)} \theta_{l(r+1)}'' + a_{2,2}^{(1,l)} \theta_{l(r+1)}' + a_{2,3}^{(1,l)} \phi_{l(r+1)}' + a_{2,1}^{(0,l)} f_{l(r+1)} = R_{2,l} \\ a_{3,3}^{(2,l)} \phi_{l(r+1)}'' + a_{3,3}^{(1,l)} \phi_{l(r+1)}' + a_{3,1}^{(0,l)} f_{l(r+1)} + a_{3,2}^{(2,l)} \theta_{l(r+1)}'' + a_{3,3}^{(0,l)} \phi_{l(r+1)} = R_{3,l} \\ a_{4,4}^{(2,l)} \chi_{l(r+1)}'' + a_{4,4}^{(1,l)} \chi_{l(r+1)}' + a_{4,4}^{(0,l)} \chi_{l(r+1)} + a_{4,1}^{(0,l)} f_{l(r+1)} + a_{4,3}^{(1,l)} \phi_{l(r+1)}' = R_{4,l} \end{array}\right\} \tag{3.6}$$

Following from the spectral quasilinearization method technique [18], the variable coefficients, as well as the boundary conditions, are written in accordance with the overlapping grid OGMDSQLM notation in (3.1), respectively.

$$\left\{\begin{array}{r} a_{1,1}^{(3,l)} = 1 + We f_{lr}'', \\ a_{1,1}^{(2,l)} = We f_{lr}''' + 2f_{lr}, a_{1,1}^{(1,l)} = -2f_{lr}', a_{1,1}^{(0,l)} = 2f_{lr}'', \\ a_{1,2}^{(0,l)} = \lambda, a_{1,3}^{(0,l)} = -\lambda Nr, a_{1,4}^{(0,l)} = -\lambda Rb, a_{2,2}^{(2,l)} = 1 + Rd, \\ a_{2,2}^{(1,l)} = PrNb\phi_{lr}' + 2PrNt\theta_{lr}' + 2Prf_{lr}, \\ a_{2,3}^{(1,l)} = PrNb\theta_{lr}', a_{2,1}^{(0,l)} = 2Pr\theta_{lr}', a_{3,3}^{(2,l)} = 1, \\ a_{3,3}^{(1,l)} = 2LePrf_{lr}, a_{3,1}^{(0,l)} = 2LePr\phi_{lr}', a_{3,2}^{(2,l)} = \dfrac{Nt}{Nb}, \\ a_{3,3}^{(0,l)} = -LeK, a_{4,4}^{(2,l)} = 1, \\ a_{4,4}^{(1,l)} = -Pe\phi_{lr}', \\ a_{4,4}^{(0,l)} = Sbf_{lr} - Pe\phi_{lr}', \\ a_{4,1}^{(0,l)} = Sb\chi_{lr}, a_{4,3}^{(1,l)} = -Pe\chi_{lr}' - Pe\chi_{lr} - PeB \end{array}\right\} \tag{3.7}$$

The boundary conditions now become;

$$\left\{\begin{array}{r} f_{l(r+1)} = 0, f_{l(r+1)}' = 1 + \gamma f_{l(r+1)}'', \theta_{l(r+1)}' = -Bt\left(1 - \theta_{l(r+1)}\right), \\ \phi_{l(r+1)} = \chi_{l(r+1)} = 1 \quad \text{at} \quad \eta = 0 \\ f_{l(r+1)}' \to 0, \theta_{l(r+1)} \to 0, \phi_{l(r+1)} \to 0, \\ \chi_{l(r+1)} \to 0, \quad \text{as} \quad \eta \to \infty \end{array}\right\} \tag{3.8}$$

Applying the Chebyshev differentiation matrix to the linearized system of equations, we write (3.1) compactly as shown in (3.8) which can further be written as a matrix equation in (3.1). The elements of the coefficient matrix are listed in (3.1).

$$\left\{\begin{array}{r} \left[a_{1,1}^{(3,l)}\mathbf{D}^3+a_{1,1}^{(2,l)}\mathbf{D}^2+a_{1,1}^{(1,l)}\mathbf{D}+a_{1,1}^{(0,l)}\mathbf{I}\right]\mathbf{F}_{l(r+1)}+ \\ a_{1,2}^{(0,l)}\mathbf{I}\boldsymbol{\Theta}_{l(r+1)}+a_{1,3}^{(0,l}\mathbf{I}\boldsymbol{\Phi}_{\mathbf{l(r+1)}} \\ +a_{1,4}^{(0,l)}\mathbf{I}\chi_{l(r+1)}=\mathbf{R}_{1,l} \\ \\ \left[a_{2,2}^{(2,l)}\mathbf{D}^2+a_{2,2}^{(1,l)}\mathbf{D}\right]\boldsymbol{\Theta}_{l(r+1)}+a_{2,3}^{(1,l)}\mathbf{D}\boldsymbol{\Phi}_{l(r+1)}+ \\ a_{2,1}^{(0,l)}\mathbf{I}\mathbf{F}_{l(r+1)}=\mathbf{R}_{2,l} \\ \\ \left[a_{3,3}^{(2,l)}\mathbf{D}^2+a_{3,3}^{(1,l)}\mathbf{D}+a_{3,3}^{(0,l)}\mathbf{I}\right]\boldsymbol{\Phi}_{l(r+1)}+a_{3,1}^{(0,l)}\mathbf{I}\mathbf{F}_{l(r+1)}+ \\ a_{3,2}^{(2,l)}\mathbf{D}^2\boldsymbol{\Theta}_{l(r+1)}=\mathbf{R}_{3,l} \\ \\ \left[\alpha_{4,4}^{(2,l)}\mathbf{D}^2+\alpha_{4,4}^{(1,l)}\mathbf{D}+\alpha_{4,4}^{(0,l)}\mathbf{I}\right]\chi_{l(r+1)}+\alpha_{4,3}^{(2,l)}\mathbf{D}^2\boldsymbol{\Theta}_{l(r+1)}+ \\ \left[\alpha_{4,1}^{(1,l)}\mathbf{D}+\alpha_{4,1}^{(0,l)}\mathbf{I}\right]\mathbf{F}_{l(r+1)}=\mathbf{R}_{4,l} \end{array}\right\} \tag{3.9}$$

$$\begin{bmatrix} A_{11} & A_{12} & A_{13} & A_{14} \\ A_{21} & A_{22} & A_{23} & A_{24} \\ A_{31} & A_{32} & A_{33} & A_{34} \\ A_{41} & A_{42} & A_{43} & A_{44} \end{bmatrix} \begin{bmatrix} \mathbf{F}_{r+1}^{l} \\ \boldsymbol{\Theta}_{r+1}^{l} \\ \boldsymbol{\Phi}_{r+1}^{l} \\ \chi_{r+1}^{l} \end{bmatrix} = \begin{bmatrix} \mathbf{R}_{1}^{l} \\ \mathbf{R}_{2}^{l} \\ \mathbf{R}_{3}^{l} \\ \mathbf{R}_{4}^{l} \end{bmatrix} \tag{3.10}$$

$$\begin{aligned} A_{11}&=\left[a_{1,1}^{(3,l)}\mathbf{D}^3+a_{1,1}^{(2,l)}\mathbf{D}^2+a_{1,1}^{(1,l)}\mathbf{D}+a_{1,1}^{(0,l)}\mathbf{I}\right], \\ A_{12}&=a_{1,2}^{(0,l)}\mathbf{I}, \quad A_{13}=a_{1,3}^{(0,l}\mathbf{I}, \quad A_{14}=a_{1,4}^{(0,l)}\mathbf{I}, \\ A_{21}&=a_{2,1}^{(0,l)}\mathbf{I}, \quad A_{22}=\left[a_{2,2}^{(2,l)}\mathbf{D}^2+a_{2,2}^{(1,l)}\mathbf{D}\right], \\ A_{23}&=a_{2,3}^{(1,l)}\mathbf{D}, \quad A_{24}=\mathbf{0} \\ A_{31}&=a_{3,1}^{(0,l)}\mathbf{I}, \quad A_{32}=a_{3,2}^{(2,l)}\mathbf{D}^2, \\ A_{33}&=\left[a_{3,3}^{(2,l)}\mathbf{D}^2+a_{3,3}^{(1,l)}\mathbf{D}+a_{3,3}^{(0,l)}\mathbf{I}\right], \quad A_{34}=\mathbf{0} \\ A_{41}&=\left[\alpha_{4,1}^{(1,l)}\mathbf{D}+\alpha_{4,1}^{(0,l)}\mathbf{I}\right], \\ A_{42}=\mathbf{0}, \quad A_{43}&=\alpha_{4,3}^{(2,l)}\mathbf{D}^2, \quad A_{44}=\left[\alpha_{4,4}^{(2,l)}\mathbf{D}^2+\alpha_{4,4}^{(1)}\mathbf{D}+\alpha_{4,4}^{(0,l)}\mathbf{I}\right] \end{aligned} \tag{3.11}$$

Applying the pseudospectral method [15] at the boundaries, (3.1) is the result.

$$\left\{\begin{array}{c} f_{r+1}(z_{N_\eta})=0, \quad \sum_{j=0}^{N_\eta} D_{N,j} f_{j(r+1)} = 1+\gamma \sum_{j=0}^{N_\eta} D_{N,j}^2 f_{j(r+1)}, \\ \sum_{j=0}^{N_\eta} D_{N,j}\theta_{j(r+1)} = -Bt(1-\theta), \phi(z_{N_\eta})=\chi(z_{N_\eta})=1 \quad \text{at} \quad \eta=0 \\ \sum_{j=0}^{N_\eta} D_{0,j} f_{j(r+1)}(z_0)\to 0, \quad \theta_{j(r+1)}(z_0)\to 0, \\ \phi_{j(r+1)}(z_0)\to 0, \quad \chi_{j(r+1)}(z_0)\to 0, \quad \text{as} \quad \eta\to\infty \end{array}\right\} \tag{3.12}$$

The matrix in (3.1) is solved iteratively on MATLAB, with the boundary conditions implemented accordingly, in the first and last rows of the diagonal sub-matrices, A_{11}, A_{22}, A_{33} and A_{44}. In order to begin the iteration, the initial solutions approximations are chosen such that they satisfy the boundary conditions of the problem (see (3.1)).

$$\begin{aligned} f_0(\eta) &= \frac{1-\exp(-\eta)}{1+\gamma} \\ \theta_0(\eta) &= \frac{Bt(\exp(-\eta))}{1+Bt} \\ \phi_0(\eta) &= \exp(-\eta) \\ \chi_0(\eta) &= \exp(-\eta) \end{aligned} \tag{3.13}$$

4. Results and discussion

To verify our numerical scheme results are compared with previously published paper. The results are found in an excellent agreement and presented in Table 1.

Table 1. Comparison of results for -$\theta'(0)$ and $-\phi'(0)$ with previous published works for: $Nr = We = \gamma = Nt = \lambda = Rb = Rd = Pe = 0; Pr = 1; Nt = Nb = 0.1; Bt = 0.5$

	$-\theta'(0)$		$-\phi'(0)$	
Le	Mustafa et al.[19]	Present results	Mustafa et al. [19]	Present results
0.4	0.310557	0.31055736	0.193614	0.19361505
2	0.305905	0.30590476	1.160300	1.16030084
10	0.303021	0.30302120	3.222890	3.22288667

4.1. **Effect of** We**.** The effect of the Williamson parameter (We) on the velocity ($f'(\eta)$) and temperature ($\theta(\eta)$) profiles was studied and the results are shown in Figure 3 and 4, respectively. Figure 3 depicts a decrease in the velocity profile as well as the momentum boundary layer thickness with increase in We. The Williamson parameter is a measure of the time fluid particles take to revert to their original configuration following a disturbance by some force [34]. Therefore, when the We is increased, the viscosity of the fluid also increases, hence the observed decrease in the fluid velocity and the momentum boundary layer thickness shrinking shown in Figure 3. In Figure 4, the temperature profile follows an increasing trend as the Williamson parameter is augmented. The increase in the viscosity of the fluid produces drag that causes the nanoparticles and the overall fluid to accumulate near the

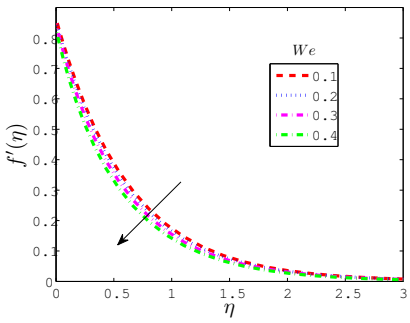

FIGURE 3. Effect of We on $f'(\eta)$.

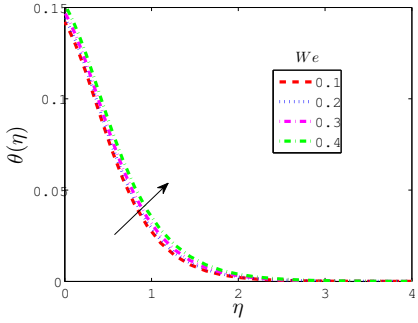

FIGURE 4. Effect of We on $\theta(\eta)$.

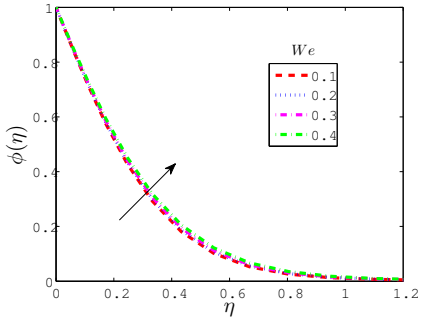

FIGURE 5. Effect of We on $\phi(\eta)$

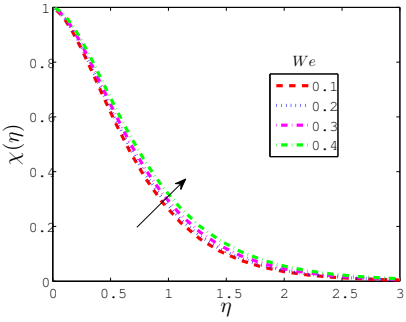

FIGURE 6. Effect of We on $\chi(\eta)$

boundary layer. Since in the vicinity of the boundary layer the temperature is higher than the ambient temperature, the fluid temperature rises as observed in Figure 4. Figures 5 and 6 show the effect of the Williamson parameter on the concentration of nanoparticles ($\phi(\eta)$) and gyrotactic microorganisms ($\chi(\eta)$), respectively. It can be seen in these figures that a rise in the value of the We causes the nanoparticle and microorganisms concentration profiles to grow. As mentioned earlier, increasing the value of the We has the effect of inducing more drag within the fluid. This drag force makes the nanoparticles as well as the microorganisms to saturate in the boundary layer.

4.2. **Effect of Nt.** Variation of the thermophoresis parameter (Nt) with temperature, nanoparticle concentration, velocity and concentration of microorganisms profiles is depicted in Figures 7, 8, 9 and 10, respectively. Thermophoresis refers to the movement of particles down a temperature gradient (that is, movement of particles from a hot surface to a cold surface) [21]. Figures 7, 8 and 10 depict increasing trends for the temperature, concentration of nanoparticles and concentration of gyrotactic microorganisms profiles, respectively, as the thermophoresis parameter is increased. On a physical perspective, the growing temperature gradient forces particulate matter in the fluid to migrate away from the hotter surface to colder ambient environment. The decrease in velocity profile in Figure 9 as the thermophoresis parameter is increased may be due to, the thermophoretic force enhancing random motion and collisions of nanoparticles and microorganisms, thus introducing additional drag in the fluid, which leads to the reduction of the overall fluid velocity.

4.3. **Effect of Nb.** Brownian motion describes the random motion of particles and or matter, often accompanied by collisions, which are also random. In this present numerical study of the Williamson nanofluid, Brownian motion is represented by the parameter Nb in the model equations. The effect of Nb on the concentration of nanoparticles, concentration of microorganisms, velocity and temperature profiles is shown in Figures 11-14. As the value of Nb is increased, the concentration distribution of

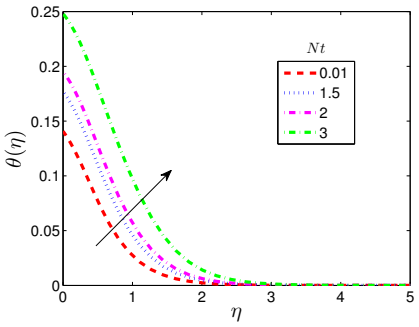

FIGURE 7. Effect of Nt on $\theta(\eta)$.

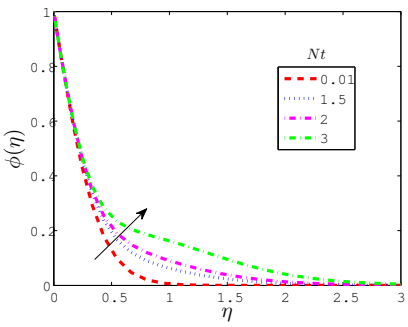

FIGURE 8. Effect of Nt on $\phi(\eta)$.

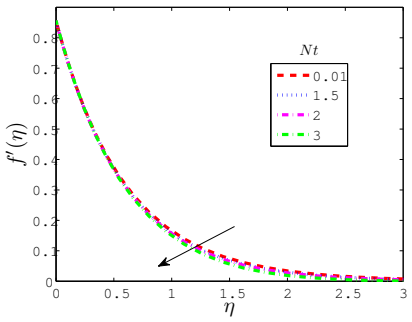

FIGURE 9. Effect of Nt on $f'(\eta)$

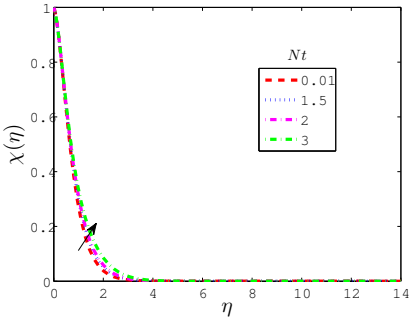

FIGURE 10. Effect of Nt on $\chi(\eta)$

nanoparticles and concentration of microorganisms profiles decreases (see Figures 11 and 12, respectively). This observed trend on the concentration of nanoparticles and concentration of microorganisms is caused by enhancement of random motion and subsequent collisions amongst nanoparticles and microorganisms as Nb is increased [35]. Furthermore, the enhanced random motion of particles slightly accelerates the fluid near the boundary layer (see Figure 13). It can be seen in Figure 14 of this present study that the thermal profile increases with an increase in the Brownian motion parameter, which is not in agreement with most studies. In addition to recent numerical models (momentum, temperature and concentration of nanoparticles equations) on MHD flow of Williamson nanofluid over a stretching sheet, this present study includes conservation of microorganisms in fluid model equations (see (2.6)).

4.4. **Slips effect.** Following consideration of the effects of velocity and temperature slips (γ and Bt (Biot number), respectively) on the velocity and temperature proles, Figures 15 and 16 are displayed. Figure 15 portrays a decreasing velocity, as well as the boundary layer as γ is increased. The rising value of the first order slip parameter (γ) introduces some drag (friction) on the fluid flow. This frictional force in turn pushes more fluid to flow past the surface, thus retardation of the fluid flow. On another note, we found that the temperature profile and the thermal boundary layer thickness increase as Bt is increased (see Figure 16). Physically, this means, the fluid's convective heat transfer at the surface improves with increasing Bt.

4.5. **Effect of Rd.** The distributions of the temperature, concentration of nanoparticles, velocity and concentration of microorganisms, with variation of the radiation parameter (Rd) are depicted in Figures 17-20, respectively. For prescribed values of the ambient fluid temperature (T_∞) and radiation absorptivity (k) in the expression of the radiation parameter ($Rd = \frac{4\sigma^* T_\infty^3}{kk^*}$), implies a decrease in the k^* (the Rosseland radiation absorptivity). This decrease in k^* causes the divergence of the radiative

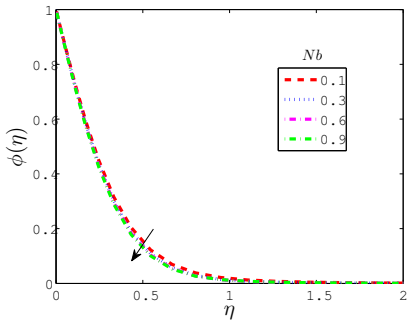

FIGURE 11. Effect of Nb on $\phi(\eta)$.

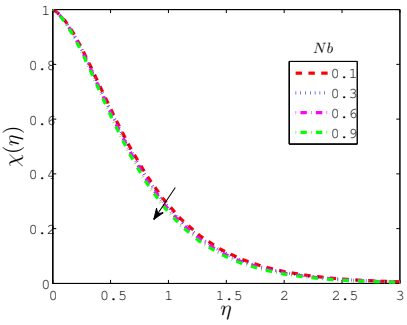

FIGURE 12. Effect of Nb on $\chi(\eta)$.

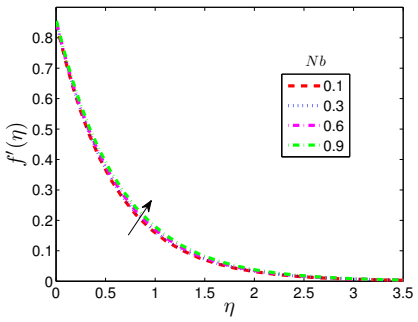

FIGURE 13. Effect of Nb on $f'(\eta)$

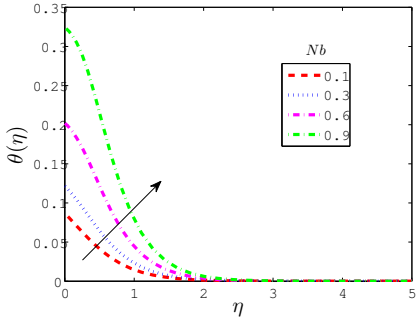

FIGURE 14. Effect of Nb on $\theta(\eta)$

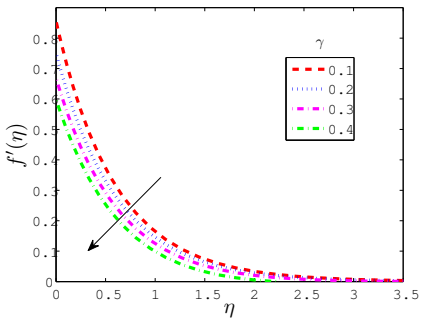

FIGURE 15. Effect of γ on $f'(\eta)$.

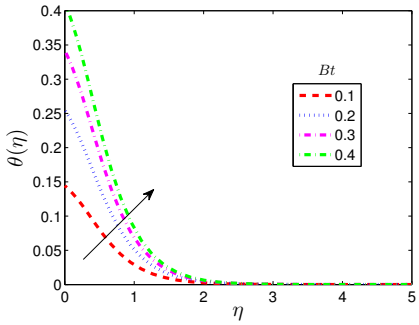

FIGURE 16. Effect of Bt on $\theta(\eta)$.

heat flux (q_r) to increase, hence the observed growth in the temperature profile and the thermal boundary layer in Figure 4.30, as the radiation parameter is increased. Furthermore, this additional heat into the fluid (in the form of radiative heat flux), enhances the buoyancy force, which in turn leads to the acceleration of the fluid and expansion of the velocity boundary layer as shown in Figure 17. Both the nanoparticles concentration and concentration of microorganisms profiles (see Figures 18 and 20, respectively) decreased with augmentation of the radiation parameter, owing to thermophoretic forces escalating the random motion of particulate matter (nanoparticles and microorganisms) in the fluid.

Effect of K. A graphic description of the effect of the chemical reaction parameter (K) on the concentration of nanoparticles and concentration of microorganisms profiles is presented in Figures 21 and 22, respectively. As shown in these figures, all the flow profiles and their boundary layer thicknesses depict a decreasing trend when the destructive chemical reaction parameter ($K > 0$) is increased. An increase in the chemical reaction parameter means the particulate matter (nanoparticles and microorganisms)

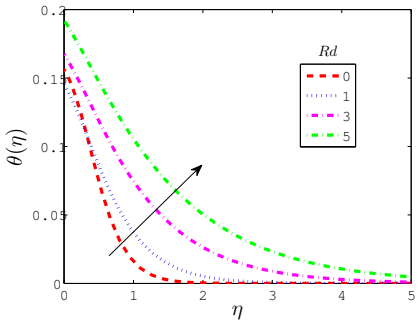

FIGURE 17. Effect of Rd on $\theta(\eta)$.

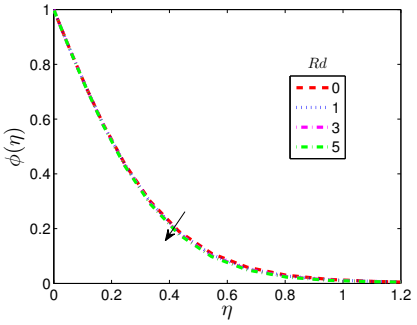

FIGURE 18. Effect of Rd on $\phi(\eta)$.

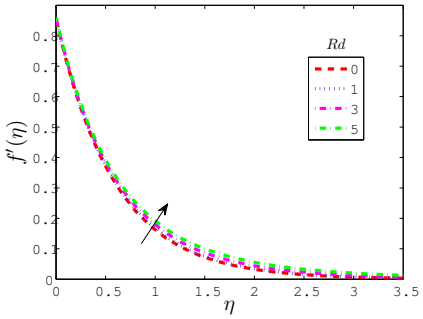

FIGURE 19. Effect of Rd on $f'(\eta)$

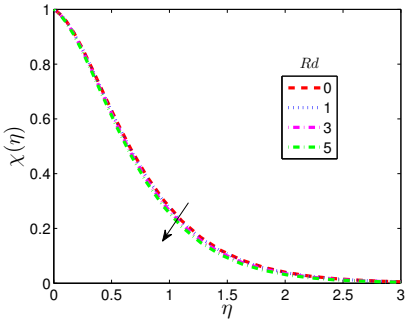

FIGURE 20. Effect of Rd on $\chi(\eta)$

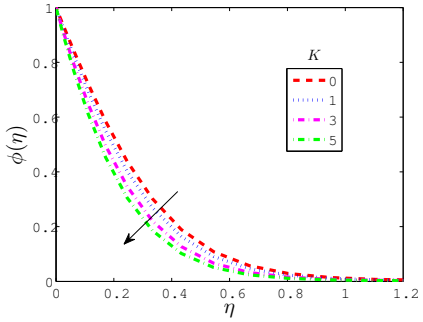

FIGURE 21. Effect of K on $\phi(\eta)$.

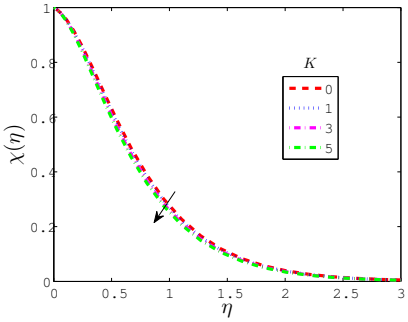

FIGURE 22. Effect of K on $\chi(\eta)$.

in the fluid decreases as it undergoes chemical transformation, hence the suppression of the concentration profile ($\phi(\eta)$) and concentration of microorganisms ($\chi(\eta)$), as well as the associated boundary layer thicknesses (see Figures 21 and 22, respectively).

4.6. **Numerical values for the local skin friction (C_f), local Nusselt number ($-\theta'(0)$) and local Sherwood number ($-\phi'(0)$).** Calculations of C_f, $-\theta'(0)$ and $-\phi'(0)$ for varying values of Rd, K and λ are displayed in Table 1. In view of the tabular results, the local Nusselt number decreases when the values of Rd and λ are augmented, while a direct proportion is observed with K. The skin friction decreases with a rise in the values of Rd and K, while it increases with the growing values of λ. When the values of Rd and K are engorged, the local Sherwood number increased in value. A declining trend on the local Sherwood number is observed for augmentation of λ values.

TABLE 2. Numerical values for the skin friction, local Nusselt number and local Sherwood number for $Rb = 0.6$; $Sb = 4$; $B = 2$; $\gamma = 0.1$; $We = 0.2$; $Nr = 0.6$; $Nb = 0.4$; $Nt = 0.2$; $Bt = 0.2$; $Le = 2$; $M = 0.5$; $Pr = 0.71$; $Pe = 0.5$;

Rd	K	λ	C_f	$-\theta'(0)$	$-\phi'(0)$
0.2	0.1	0.5	2.40432	0.13267	0.97768
0.5	0.1	0.5	2.39258	0.12782	0.99170
0.8	0.1	0.5	2.38301	0.12373	1.00288
0.6	0.2	0.5	2.38485	0.12672	1.10388
0.6	0.4	0.5	2.37861	0.12713	1.28735
0.6	0.7	0.5	2.37228	0.12746	1.51542
0.6	0.1	0.3	2.35499	0.12684	1.00804
0.6	0.1	0.5	2.38919	0.12639	0.99568
0.6	0.1	0.8	2.44749	0.12535	0.97393

5. Conclusion

A steady, incompressible Williamson nanofluid with suspension of gyrotactic microorganisms on a non-porous radially stretching sheet under the influence of a magnetic field has been studied. Following similarity transformations, the coupled system of governing nonlinear partial differential equations was reduced to a system of nonlinear ordinary differential equations. The effects of various parameters on velocities, temperature, concentration, and density of motile microorganisms were studied graphically. In addition, engineering insights were examined by computations of numerical values of the local skin friction, local Nusselt number and local Sherwood number and presented in tabular format. The highlights of the study are:

- The velocity decreases with rise in values of the Williamson parameter.
- The skin friction increases as the values of Williamson parameter and mixed convection parameter increase.
- The temperature increases with the rise in values of radiation and Williamson parameters.
- Increasing the destructive chemical reaction parameter reduces the concentration of nanoparticles and gyrotactic microorganisms.
- A rise in the value of the first order slip parameter augments the gyrotactic microorganisms concentration.
- The local Nusselt number decreases when the values of radiation parameter (Rd) and mixed convection parameter (λ) are augmented, while it increases with the chemical reaction parameter (K).
- The skin friction decreases with a rise in the values of Rd and K, while it increases with the growing values of λ.
- When the values of Rd and K are engorged, the local Sherwood number increased in value.
- A declining trend on the local Sherwood number is observed for augmentation of λ values.

Statements and Declarations

The authors declare that they have no conflict of interest.

References

[1] S. M. Atif, S. Hussain, and M. Sagheer. Magnetohydrodynamic stratified bioconvective flow of micropolar nanofluid due to gyrotactic microorganisms. *AIP Advances*, 9(2):025208, 2019.

[2] M. S. Ayano, V. M. Magagula, and J. S. Mathunjwa. Spectral local linearisation method for mhd casson fluid on stratified bioconvective porous medium flow due to gyrotactic microorganisms. *Heat Transfer*, 50(2):1371-1391, 2021.
[3] K. Bing, A. Hussanan, M. K. A. Mohamed, and M. Z. Salleh. Heat and mass transfer analysis on flow of williamson nanofluid with thermal and velocity slips. *Propulsion and Power Research*, 8(3):243-252, 2019.
[4] J. Buongiorno. Convective transport in nanofluids. *Journal of Heat Transfer*, 128(3):240-250, 2005.
[5] S. U. S. Choi and J. A. Eastman. Enhancing thermal conductivity of fluids with nanoparticles. *Technical report*, Argonne National Lab. (ANL), 1995.
[6] L. J. Crane. Flow past a stretching plate. *Journal of Applied Mathematics and Physics*, 21:645-647, 1970.
[7] N. A. Hill and T. J. Pedley. Bioconvection. *Fluid Dynamics Research*, 37(1-2):1-20, 2005.
[8] K. H. Hosseinzadeh and D. D. Ganji. Investigation of nano-bioconvective fluid motile microorganism and nanoparticle flow by considering mhd and thermal radiation. *Informatics in Medicine Unlocked*, 21:100426, 2020.
[9] W. Ibrahim and D. Gamachu. Nonlinear convection flow of williamson nanofluid past a radially stretching surface. *AIP Advances*, 9(8):085026, 2019.
[10] W. Ibrahim and M. Negera. Viscous dissipation effect on williamson nanofluid over stretching/shrinking wedge with thermal radiation and chemical reaction. *Journal of Physics Communications*, 4(4):045015, 2020.
[11] T. T. Medjo. Fixed-point iteration method for nonlinear robust control problems in fluid mechanics, *Numerical Functional Analysis and Optimization*, 23:7-8, 2002.
[12] V. Kumaran, A. K. Banrejee, A. V. Kumar, and I. Pop. Unsteady mhd flow and heat transfer with viscous dissipation past a stretching sheet. *International Communications in Heat and Mass Transfer*, 38(3):335–359, 2011.
[13] V. Kumaran, A. V. Kumar, and I. Pop. Transition of mhd boundary layer flow past a stretching sheet. *Communications in Nonlinear Science and Numerical Simulation*, 15(2):300–311, 2010.
[14] M. Yu, X. Nie, G. Yang, G. et al , Fixed-Point Fluid structure interaction analysis based on geometrically exact approach. *Scientific Reports*, 10:10322, 2020.
[15] M. P. Mkhatshwa, S. S. Motsa, M. S. Ayano, and P. Sibanda. Overlapping multi-domain spectral method for non-darcian mixed convection chemically reacting flow of micropolar fluid over a flat plate in a porous media. *Journal of Applied Analysis and Computation*, 11(1):113–137, 2021.
[16] R. A. Mohamed, S. M. Abo-Dahab, and M. S. Soliman. Effects of nonlinear thermal radiation and heat generation/absorption on magnetohydrodynamic (mhd) carreau nanofluid flow on a nonlinear stretching surface through a porous medium. *Journal of Nanofluid*, 11(6):845–856, 2022.
[17] H. Mondal and D. Pal. Effects of soret dufour, chemical reaction and thermal radiation on mhd non-darcy unsteady mixed convective heat and mass transfer over a stretching sheet. *Communications in Nonlinear Science and Numerical Simulation*, 16(4):1942–1958, 2011.
[18] S. S. Motsa, P. Sibanda, and S. Shateyi. On a new quasilinearization method for systems on nonlinear boundary value problems. *Mathematical Methods in Applied Sciences*, 34(34):1406–1413, 2011.
[19] M. Mustafa, T. Hayat, and A. Alsaedi. Axisymmetric flow a nanofluid over a radially stretching sheet with convective boundary conditions. *Current Nanoscience*, 8(3):328–334, 2012.
[20] S. Nadeem, S. T. Hussain, and C. Lee. Flow of a williamson fluid over a stretching sheet. *Brazilian Journal of Chemical Engineering*, 30(3):619–625, 2013.
[21] R. Piazza. Thermophoresis: moving particles with thermal gradients. *Soft Matter*, 4(9):1740–1744, 2008.
[22] B. Rana et al. Swimming of microbes in blood flow of nanobioconvective williamson fluid. *Thermal Science and Engineering Progress*, 25:101018, 2021.
[23] J. Raza, F. Mebarek-Oudina, and B. Mahanthesh. Magnetohydrodynamic flow of nano williamson fluid generated by stretching plate with multiple slips. *Multidiscipline Modeling in Materials and Structures*, 15(5), 2019.
[24] R. Saidura, K. Y. Leong, and H. A. Mohammad. A review on applications and challenges of nanofluids. *Renewable and Sustainable Energy Reviews*, 15(3):1646–1668, 2011.
[25] J. Sarkar and A. Adil. A review in hybrid nanofluids: Recent research, development and application. *Renewable and Sustainable Energy Reviews*, 43:164–177, 2015.
[26] H. M. Shawky, N. T. M. Eldabe, K. A. Kamel, and E. A. Abd-Aziz. Mhd flow with heat and mass transfer of williamson nanofluid over stretching sheet through porous medium. *Microsystem Technologies*, 25:1155–1169, 2019.
[27] K. C. Shobha and B. P. Mallikarjun. Effect of nonlinear thermal radiation on flow of williamson nanofluid in a vertical porous channel with heat source or sink by using adomian decomposition method. *Journal of Nanofluid*, 11(1):39–47, 2022.
[28] D. R. Smith. The cauchy stress tensor. *Introduction to Continuum Mechanics-After Truesdell and Noll*, pages 143–162. 1993.
[29] J. Smith et al. Fixed point methods for nanofluid dynamics. *Journal of Computational Fluid Dynamics*, 25(2):123–135, 2018.

[30] K. Subbarayudu, S. Suneetha, and P. B. A. Reddy. The assessment of time dependent flow of williamson fluid with radiative blood flow against a wedge. *Propulsion and Power Research*, 9(1):87–99, 2020.

[31] R. Tamizharasi and V. Kumaran. Pressure in mhd/brinkman flow past a stretching sheet. *Communications in Nonlinear Science and Numerical Simulation*, 16(12):4671–4681, 2011.

[32] X.-Q. Wang and A. S. Mujumdar. Heat transfer characteristics of nanofluids: a review. *International Journal of Thermal Sciences*, 46(1):1–19, 2007.

[33] H. Waqas, M. Imran, S. Hussain, F. Ahmad, I. Khan, K. S. Nisar, A. O. Almatroud. Numerical simulation for bioconvection effects on mhd flow of oldroyd-b nanofluids in a rotating frame stretching horizontally. *Mathematics and Computers in Simulation*, 178:166–182, 2020.

[34] R. V. Williamson. The Flow of Pseudoplastic Materials. *Industrial and Engineering Chemistry*, 21(11):1108–1111, 1929.

[35] I. Wubshet and G. Dachasa. Finite element method solution of mixed convection flow of williamson nanofluid past a radially stretching sheet. *Heat Transfer*, 49(2):800–822, 2020.

[36] S. Deparis, M. A. Fernandez and L Formaggia. Acceleration of a Fixed-Point algorithm for fluid-structure interaction using transpiration conditions. *ESAIM: Math Mod and Numerical Analysis*, 37(4):601-616, 2003.